Int. J. Radiation Oncology Biol. Phys., Vol. 75, No. 3, pp. 782–790, 2009

0360-3016/09/$–see front matter

ELSEVIER

doi:10.1016/j.ijrobp.2008.11.031

ASTRO Online CME

CLINICAL INVESTIGATION Rectum

BIOLOGICAL IMAGE-GUIDED RADIOTHERAPY IN RECTAL CANCER: CHALLENGES AND PITFALLS

Sarah Roels, M.D.,* Pieter Slagmolen,† Johan Nuyts, Ph.D.,‡ John A. Lee, Ph.D.,§ Dirk Loeckx, Ph.D.,† Frederik Maes, Ph.D.,† Vincent Vandecaveye, M.D.,‖ Sigrid Stroobants, M.D., Ph.D.,‡ Nadine Ectors, M.D., Ph.D.,¶ Freddy Penninckx, M.D., Ph.D.,# and Karin Haustermans, M.D., Ph.D.*

*Department of Radiation Oncology, Leuven Cancer Institute, ‡Department of Nuclear Medicine, ‖Department of Radiology, ¶Department of Pathology, and #Department of Abdominal Surgery, University Hospital Leuven, Leuven, Belgium; †Medical Image Computing, ESAT/Radiology, Medical Imaging Center, Catholic University Leuven, Leuven, Belgium; and §Center for Molecular Imaging and Experimental Radiotherapy, Université Catholique de Louvain, Brussels, Belgium

Purpose: To investigate the feasibility of integrating multiple imaging modalities for image-guided radiotherapy in rectal cancer.

Patients and Methods: Magnetic resonance imaging (MRI) and fluorodeoxyglucose positron emission tomography/computed tomography (FDG-PET/CT) were performed before, during, and after preoperative chemoradiotherapy (CRT) in patients with resectable rectal cancer. The FDG-PET signals were segmented with an adaptive threshold-based and a gradient-based method. Magnetic resonance tumor volumes (TVs) were manually delineated. A nonrigid registration algorithm was applied to register the images, and mismatch analyses were carried out between MR and FDG-PET TVs and between TVs over time. Tumor volumes delineated on the images after CRT were compared with the pathologic TV.

Results: Forty-five FDG-PET/CT and 45 MR images were analyzed from 15 patients. The mean MRI and FDG-PET TVs showed a tendency to shrink during and after CRT. In general, MRI showed larger TVs than FDG-PET. There was an approximately 50% mismatch between the FDG-PET TV and the MRI TV at baseline and during CRT. Sixty-one percent of the FDG-PET TV and 76% of the MRI TV obtained after 10 fractions of CRT remained inside the corresponding baseline TV. On MRI, residual tumor was still suspected in all 6 patients with a pathologic complete response, whereas FDG-PET showed a metabolic complete response in 3 of them. The FDG-PET TVs delineated with the gradient-based method matched closest with pathologic findings.

Conclusions: Integration of MRI and FDG-PET into radiotherapy seems feasible. Gradient-based segmentation is recommended for FDG-PET. Spatial variance between MRI and FDG-PET TVs should be taken into account for target definition.

Rectal cancer, Image-guided radiotherapy, Tumor delineation, Tumor evolution, FDG-PET/CT, MRI.

INTRODUCTION

Rectal cancer patients at high risk for local recurrence could benefit from higher radiotherapy (RT) doses, provided they are associated with an acceptable toxicity (1–3). This can be achieved with three-dimensional (3D) conformal and intensity-modulated RT, which allow optimal dose distributions but require a precise definition and an accurate location of the target volume. Various imaging modalities that give anatomic and functional information have been tested for definition of the tumor volume (TV) for various tumor sites (4–8). Computed tomography (CT) generally has a poor soft-tissue contrast, which makes it less reliable for accurate delineation of the TV (6, 9). Nonetheless, CT is needed for planning and subsequent verification of radiation treatment because CT provides electron densities. Magnetic resonance imaging (MRI) generally presents better soft-tissue contrast than CT. Functional imaging is a promising tool for the detection of malignant tissue or specific areas in the tumor that appear more radioresistant and that can be targeted with nonuniform customized dose distributions (10).

Note—An online CME test for this article can be taken at http://asro.astro.org under Continuing Education.

Reprint requests to: Karin Haustermans, M.D., Ph.D., Leuven Cancer Institute, University Hospital Leuven, Herestraat 49, 3000 Leuven, Belgium. Tel: (+32) 16-346902; Fax: (+32) 16-346901; E-mail: Karin.Haustermans@uzleuven.be

This work was supported in part by a grant from Varian Medical Systems and by a grant from BIOCARE. S.R. is supported by a grant from the Belgian Foundation Against Cancer (Katholieke Universiteit Leuven: No. SCIE2003-23 [ZKB2747]). S.S. is supported by a grant from the Fonds Wetenschappelijk Onderzoek (FWO) – Vlaanderen, Credit G.0177.04. K.H. is supported by a fundamental clinical mandate of the FWO.

Conflict of interest: none.

Received April 16, 2008, and in revised form Nov 4, 2008. Accepted for publication Nov 5, 2008.

Positron emission tomography (PET) with fluorodeoxyglucose (^{18}F-FDG) is most widely used to detect regions with a high metabolic activity. Combined FDG-PET/CT imaging improves accuracy compared with either of its individual components (11, 12). The potential use of FDG-PET/CT in RT planning has been addressed for various tumor sites (13), including rectal cancer (6, 14, 15).

Optimized tumor imaging might be of little benefit for the current treatment of rectal cancer, whereby a uniform dose is prescribed to the whole posterior pelvis. However, it becomes more important when ''dose painting'' to the gross tumor volume (GTV) or relevant biologic regions is aimed at to increase tumor response (16).

More recently, repeated imaging during RT has been investigated to track geometric and biologic changes of the tumor and adapt the treatment plan accordingly (17).

Introducing multiple imaging modalities at various time points during the treatment necessitates exact registration of the images to a common reference image, to accurately (re)plan the treatment and (re)calculate time-adjusted dose distributions.

The main purpose of this study was to investigate the use of FDG-PET/CT and MRI for target definition in rectal cancer. Two different FDG-PET segmentation algorithms were tested, and posttreatment FDG-PET and MRI TVs were compared with the pathologic TV. We also assessed the spatial distribution of FDG-PET- and MRI-defined TVs. Finally, this study evaluated the quantitative and spatial evolution of the MRI and FDG-PET TVs during preoperative chemoradiotherapy (CRT).

PATIENTS AND METHODS

Patient selection

Between May 2005 and August 2007, 15 patients comprising 11 men (mean age, 63 years; range, 48–82 years) and 4 women (mean age, 62 years; range, 49–77 years) were enrolled in the study. All patients had biopsy-proven resectable adenocarcinoma of the rectum, clinical stage T2/3-N1/2M0 on MRI and/or rectal endosonography. All patients were treated with a long course of CRT, consisting of 25 fractions of 1.8 Gy, 5 days per week for 5 weeks, in combination with a continuous infusion of 5-fluorouracil (225 mg/m^2). Radiotherapy was delivered through two lateral beams and one posterior beam. During simulation and treatment, patients were positioned in the prone position on a belly board. Six to 8 weeks after completion of CRT, patients underwent radical rectum resection with a total or partial mesorectal excision.

Image acquisition

Imaging was performed with MRI and FDG-PET/CT at three time points: before the start of CRT, after 10 fractions of RT, and before surgery (i.e., 6–8 weeks after the end of CRT). Magnetic resonance imaging was carried out within 24 h from the FDG-PET/CT.

FDG-PET/CT

The FDG-PET/CT images were acquired with a Siemens Biograph 2 scanner (Siemens, Erlangen, Germany) (4 patients) or with a Siemens HiRez Biograph scanner (11 patients). The transaxial and axial PET resolution for the HiRez Biograph PET camera were 4.6 mm at 1 cm and 5.8 mm at 10 cm from the center. The Biograph 2 PET camera has a transaxial resolution of 6.3 mm and 7.4 mm and an axial resolution of 5.8 mm and 7.1 mm at 1-cm and 10-cm source distance, respectively.

Patients were asked to fast for 6 h before the examination. A dose between 282 MBq (minimum) and 404 MBq (maximum) ^{18}F-FDG was administered i.v. [injected dose = (body weight × 4) + 20]. Each examination consisted of a spiral CT scan followed by a PET acquisition in the caudocranial direction over the same anatomic extent (from L4 to the buttock folds). Each FDG-PET/CT scan before treatment was performed using a high dose CT with i.v. contrast, because these images were used for RT treatment planning. Computed tomography scans during RT were obtained with low doses and without i.v. contrast. Immediately after the CT scan, the emission scan was obtained in 3D mode in two or three bed positions, with a scan time of 4 min per bed position. All PET/CT acquisitions were performed with the patient in treatment position. The PET data were reconstructed using an ordered subset expectation maximization algorithm and attenuation correction derived from CT data (18). Total acquisition time was approximately 45 min.

Magnetic resonance imaging

All patients were positioned supine on the MRI table because this position resulted in better image quality, owing to less patient movement and fewer breathing artefacts. Rectal contrast was used to improve tumor visualization. Images were obtained with a 1.5-T MRI system (Siemens Magnetom Sonata), using a dedicated surface coil. For each patient, T2-weighted turbo spin-echo images were obtained in the sagittal, transaxial, and coronal planes. In addition, T1-weighted transaxial sequences were obtained. Total acquisition time was approximately 20 min.

Delineation of tumor volumes

The FDG-PET signals were automatically processed, and metabolically active regions in the tumor were outlined by use of an adaptive threshold method based on the signal-to-background ratio (SBR) (19) and a gradient-based segmentation method (20).

The FDG-PET images from the Biograph 2 were first processed with an edge-preserving bilateral filter and then with a constrained deconvolution algorithm, which restored the gradient–intensity peaks. The FDG-PET images from the HiRez Biograph scanner

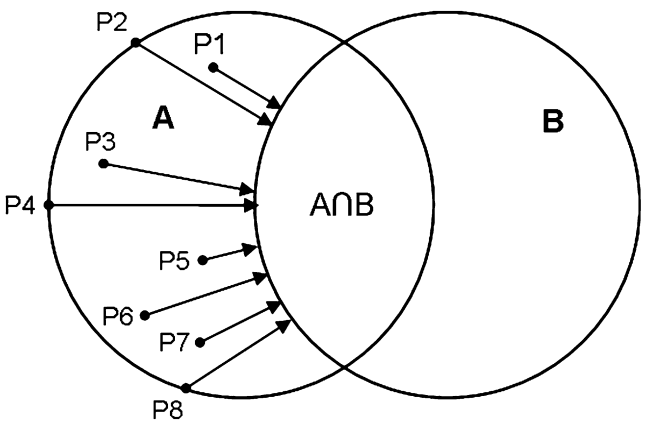

Fig. 1. Maximum value of shortest distances between A-B volume and A∩B: the maximum of all shortest distances of all points inside A-B volume (P1, 2…Pn) to the intersection (A∩B) (arrow from P4). Mean value of shortest distances between A-B volume and A∩B: mean of all shortest distances of all points inside A-B volume (P1, P2…Pn) to the intersection (A∩B).